On the solubility of rare earths in M-type $SrFe_{12}O_{19}$ hexaferrite compounds

2008 J. Phys.: Condens. Matter 20 175203

(http://iopscience.iop.org/0953-8984/20/17/175203)

J. Phys.: Condens. Matter **20** (2008) 175203 (9pp) doi:10.1088/0953-8984/20/17/175203

On the solubility of rare earths in M-type $SrFe_{12}O_{19}$ hexaferrite compounds

L Lechevallier[1,3], J M Le Breton[1], A Morel[2] and P Tenaud[2]

[1] Groupe de Physique des Matériaux, UMR CNRS 6634, Université de Rouen avenue de l'Université BP 12, 76801 Saint Etienne du Rouvray, France
[2] UGIMAG, 38830 Saint Pierre d'Allevard, France

E-mail: luc.lechevallier@univ-rouen.fr

Received 10 December 2007, in final form 4 February 2008
Published 3 April 2008
Online at stacks.iop.org/JPhysCM/20/175203

Abstract

$Sr_{1-x}RE_xFe_{12}O_{19}$ and $Sr_{1-x}RE_xFe_{12-x}Co_xO_{19}$ ($x = 0$–0.4 and RE = Pr, Nd) M-type hexaferrite powders were produced by a conventional ceramic process. Structural investigations made by x-ray diffraction and Mössbauer spectrometry reveal that the solubility of the rare earth ion in the M-type phase depends on both the nature of the rare earth and the presence of Co. The solubility of Pr in the M-type phase is higher than the solubility of Nd, and the presence of Co increases the solubility of the rare earth ion. These results were interpreted in the frame of the published literature. It appears that only light rare earths can enter the M-type structure, with a solubility that is related to the shape of the 4f electronic charge distribution and to its surroundings in the crystal structure. Rare earth ions are located in the Sr^{2+} site, whose surroundings favour an oblate electronic distribution. Co^{2+} ions modify the surroundings of the Sr^{2+} site, improving the introduction of rare earth ions with oblate electronic distribution.

1. Introduction

Since the discovery of the M-type $BaFe_{12}O_{19}$ and $SrFe_{12}O_{19}$ hexagonal ferrites, and because of the large market share that they still have, numerous studies have been made in the last 10 years to improve their magnetic properties. A significant improvement has been obtained in $SrFe_{12}O_{19}$ hexaferrites by the combined substitution of La^{3+} in the Sr^{2+} site and Co^{2+} in Fe^{3+} sites, leading to a chemical formula of $Sr_{1-x}La_xFe_{12-x}Co_xO_{19}$ [1, 2]. These improvements are related to the increase of the intrinsic magnetic properties of the modified M-type phase, in particular to a drastic change of the magneto-crystalline anisotropy field [3]. A further improvement could be obtained by using a rare earth ion, which carries a magnetic moment, instead of a La^{3+} ion. This has been studied for the Sm^{3+} ion [4, 5], Nd^{3+} ion [6, 7] and Gd^{3+} ion [8]. However, the solubility of rare earth ions in Sr-hexaferrites is very low and their introduction leads to the formation of secondary phases which must be avoided in order to obtain permanent magnets with optimal properties [7, 8]. The increase of the solubility of rare earth ions in Sr-hexaferrites is the object of an important research effort to obtain highly substituted single phase samples which could have magnetic properties better than those of La–Co substituted hexaferrites.

M-type ferrites crystallize in a hexagonal structure with 64 ions per unit cell on 11 different symmetry sites ($P6_3/mmc$ space group). The 24 Fe^{3+} atoms are distributed over five distinct sites: three octahedral sites (12k, 2a and $4f_2$), one tetrahedral ($4f_1$) site and one bipyramidal site (2b). The magnetic structure is ferrimagnetic with five different sublattices: three parallel (12k, 2a and 2b) and two antiparallel ($4f_1$ and $4f_2$) [9].

The cationic distribution of Co^{2+} in the M-type structure was recently investigated in $Sr_{1-x}La_xFe_{12-x}Co_xO_{19}$ hexagonal ferrites prepared by a ceramic process. It has been shown that Co^{2+} ions have a marked preference for octahedral sites, being substituted for Fe^{3+} in both $4f_2$ and 2a sites [10, 11]. The fact that Co^{2+} is present in both parallel (2a) and antiparallel ($4f_2$) magnetic sites explains the fact that the saturation magnetization does not vary significantly with x, in agreement with magnetization measurements [1, 2].

In this paper, we present the results of the structural investigation of $Sr_{1-x}RE_xFe_{12}O_{19}$ and $Sr_{1-x}RE_xFe_{12-x}Co_xO_{19}$ ($x = 0$–0.4 and RE = Pr, Nd) hexaferrite powders. The

[3] Address for correspondense: Groupe de Physique des Matériaux, UMR 6634 CNRS, Université de Rouen Site universitaire du Madrillet avenue de l'Université, BP 12, 76801 Saint Etienne du Rouvray Cedex, France.

results are presented, compared and discussed in the frame of the published literature. The solubility of the rare earth ion is interpreted taking into account the surroundings of the Sr^{2+} ion site and the nature of the rare earth ion. The influence of the presence of Co^{2+} on the solubility of Pr^{3+} and Nd^{3+} is discussed in that frame.

2. Experimental details

$Sr_{1-x}RE_xFe_{12}O_{19}$ and $Sr_{1-x}RE_xFe_{12-x}Co_xO_{19}$ (RE = Pr, Nd) samples with different substitution ratios (x = 0–0.4) were produced according to a conventional ceramic process.

For the Co-free samples, a mixture of α-Fe_2O_3, $SrCO_3$ and Nd_2O_3 (or Pr_2O_3) powders was pressed into discs, with 12% water (which acts as a binder). The density of the discs is 2.5 g cm^{-3}. The discs were then calcined at 1250 °C for 2 h in air, and the M-type phase was synthesized according to the following reactions:

$$(1-x)SrCO_3 + 6Fe_2O_3 + \frac{x}{2}Nd_2O_3 \rightarrow Sr_{1-x}Nd_xFe_{12}O_{19} + (1-x)CO_2 + \frac{x}{4}O_2$$

$$(1-x)SrCO_3 + 6Fe_2O_3 + \frac{x}{2}Pr_2O_3 \rightarrow Sr_{1-x}Pr_xFe_{12}O_{19} + (1-x)CO_2 + \frac{x}{4}O_2.$$

For the Co-containing samples, the process was the same with a mixture of α-Fe_2O_3, $SrCO_3$, Co_3O_4 and Nd_2O_3 (or Pr_2O_3) powders. The corresponding reactions are:

$$(1-x)SrCO_3 + \frac{(12-x)}{2}Fe_2O_3 + \frac{x}{2}Nd_2O_3 + \frac{x}{3}Co_3O_4 \rightarrow Sr_{1-x}Nd_xFe_{12-x}Co_xO_{19} + (1-x)CO_2 + \frac{x}{6}O_2$$

$$(1-x)SrCO_3 + \frac{(12-x)}{2}Fe_2O_3 + \frac{x}{2}Pr_2O_3 + \frac{x}{3}Co_3O_4 \rightarrow Sr_{1-x}Pr_xFe_{12-x}Co_xO_{19} + (1-x)CO_2 + \frac{x}{6}O_2.$$

The calcined powders were characterized by x-ray diffraction (XRD) and Mössbauer spectrometry. X-ray diffraction analysis was performed by reflection with a Bruker D8 system in Bragg–Brentano θ–2θ geometry. The x-ray generator was equipped with a Co anticathode, using Co (Kα) radiation (λ = 0.178 897 nm).

Mössbauer spectrometry analysis was performed at room temperature in transmission geometry using a ^{57}Co source in a rhodium matrix. The isomer shift (relative to metallic α-Fe at room temperature), quadrupolar splitting and hyperfine field are denoted δ, Δ and B, respectively. Estimated errors for the hyperfine parameters originate from the statistical errors σ given by the fitting program [12], taking 3σ.

The Mössbauer contribution of the M-type phase is fitted with five components that correspond to the five different sites of the M-type crystal structure, i.e. the 12k, $4f_1$, $4f_2$, 2a and 2b sites. Preliminary fittings revealed that the relative intensities deviate from the crystallographic occupancy, and for the spectra of the Co-free samples the proportions 12:4:4:2:1.2 for the 12k, $4f_1$, $4f_2$, 2a and 2b sites, respectively, were used. Such a deviation is generally observed in the M-type hexaferrites,

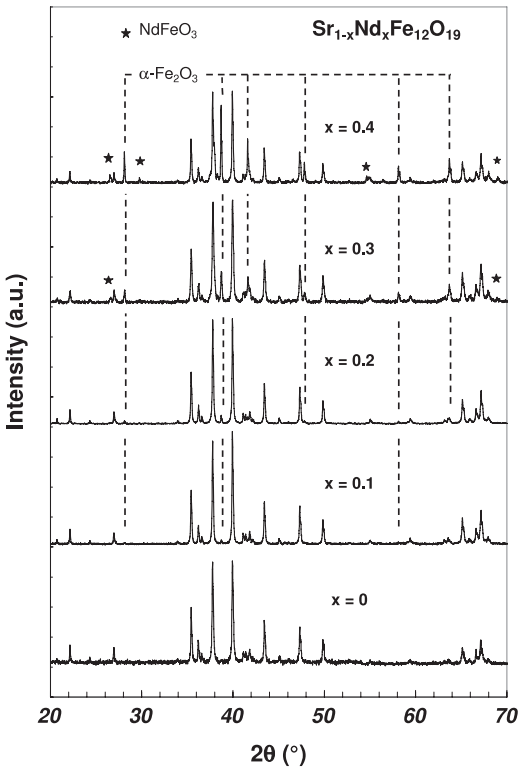

Figure 1. X-ray diffraction patterns of the $Sr_{1-x}Nd_xFe_{12}O_{19}$ powders. The non-indexed peaks are those of the M-type phase.

and can be attributed to anisotropic f-factors [13], to stacking faults [13] or to the pronounced anisotropy of the 2b site [14]. In Co-containing samples, the contribution of the M-type phase was fitted by taking into account the presence of Co^{2+} ions in both $4f_2$ and 2a sites, as for $Sr_{1-x}La_xFe_{12-x}Co_xO_{19}$ powders [10, 11, 15], in agreement with the literature.

3. Results and discussion

3.1. Structural investigation and phase analysis

3.1.1. X-ray diffraction. The x-ray diffraction patterns of $Sr_{1-x}Nd_xFe_{12}O_{19}$, $Sr_{1-x}Nd_xFe_{12-x}Co_xO_{19}$, $Sr_{1-x}Pr_xFe_{12}O_{19}$ and $Sr_{1-x}Pr_xFe_{12-x}Co_xO_{19}$ samples are shown in figures 1–4, respectively. The x-ray diffraction analyses reveal that, in all the patterns, the main peaks correspond to the hexagonal M-type phase (JCPDS file 80-1198).

For the x = 0 powder, no extra peak related to secondary phases is observed in the pattern, indicating that the starting powder is single phase. As x increases, and for each series of powders, extra peaks appear, and their intensities increase with x. Table 1 shows for each sample the nature of the phases corresponding to the extra peaks observed in the patterns.

The presence of the α-Fe_2O_3 (JCPDS file 87-1164) phase is related to an incomplete calcination reaction. The presence of $NdFeO_3$ (JCPDS file 88-0477), $PrFeO_3$ (JCPDS file 74-1472) and $CoFe_2O_4$ (JCPDS file 79-1744) phases indicates that all the Nd, Pr and Co atoms do not enter the M-type phase when the substitution rate x is too high. However, as

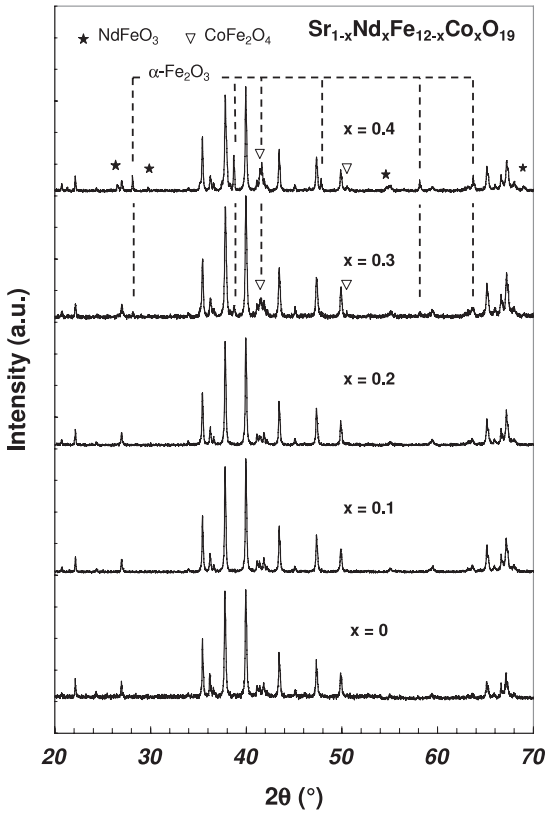

Figure 2. X-ray diffraction patterns of the $Sr_{1-x}Nd_xFe_{12-x}Co_xO_{19}$ powders. The non-indexed peaks are those of the M-type phase.

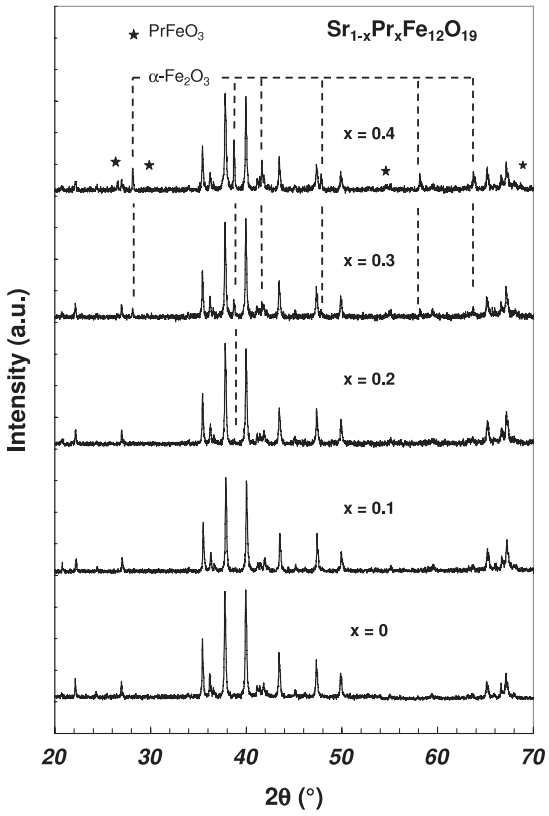

Figure 3. X-ray diffraction patterns of the $Sr_{1-x}Pr_xFe_{12-x}O_{19}$ powders. The non-indexed peaks are those of the M-type phase.

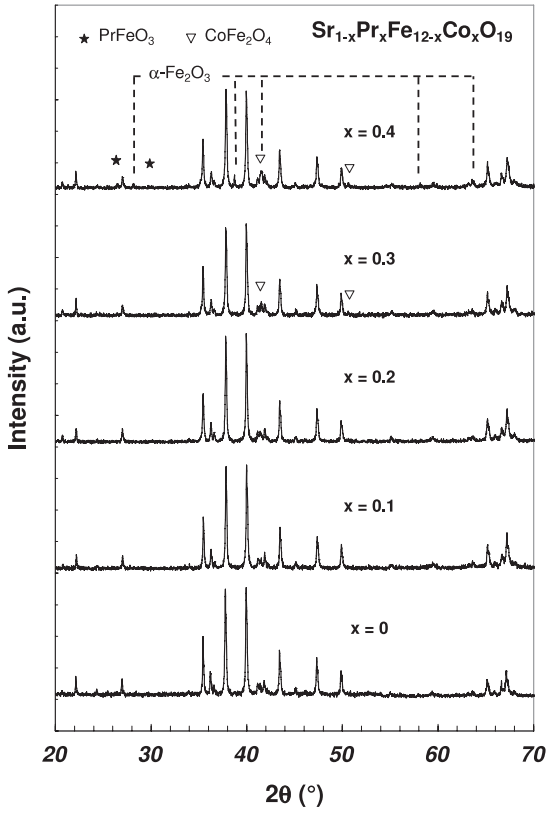

Figure 4. X-ray diffraction patterns of the $Sr_{1-x}Pr_xFe_{12-x}Co_xO_{19}$ powders. The non-indexed peaks are those of the M-type phase.

Table 1. Nature of the extra phases identified by x-ray diffraction for each investigated sample.

	$x = 0$	$x = 0.1$	$x = 0.2$	$x = 0.3$	$x = 0.4$
Nd	—	α-Fe_2O_3 (traces)	α-Fe_2O_3	α-Fe_2O_3 $NdFeO_3$	α-Fe_2O_3 $NdFeO_3$
Pr	—	—	α-Fe_2O_3 (traces)	α-Fe_2O_3	α-Fe_2O_3 $PrFeO_3$
Nd–Co	—	—	—	α-Fe_2O_3 $CoFe_2O_4$ (traces)	α-Fe_2O_3 $CoFe_2O_4$ $NdFeO_3$
Pr–Co	—	—	—	$CoFe_2O_4$ (traces)	α-Fe_2O_3 $CoFe_2O_4$ $PrFeO_3$

the proportion of extra phases is systematically lower in Co-containing powders than in Co-free powders, this indicates that for the same calcination conditions, the presence of Co improves the calcination reaction and thus increases the solubility of the rare earth in the M-type phase. Moreover, for the same composition, it appears that the proportion of extra phases is lower in Pr-containing powders than in Nd-containing powders, suggesting that the substitution rate of Pr in the M-type hexagonal phase is higher than that of Nd.

3.1.2. Mössbauer spectrometry. The room temperature Mössbauer spectra of the $Sr_{1-x}Nd_xFe_{12}O_{19}$, $Sr_{1-x}Nd_xFe_{12-x}Co_xO_{19}$, $Sr_{1-x}Pr_xFe_{12}O_{19}$, and $Sr_{1-x}Pr_xFe_{12-x}Co_xO_{19}$ samples are shown in figures 5–8 respectively. The four series of

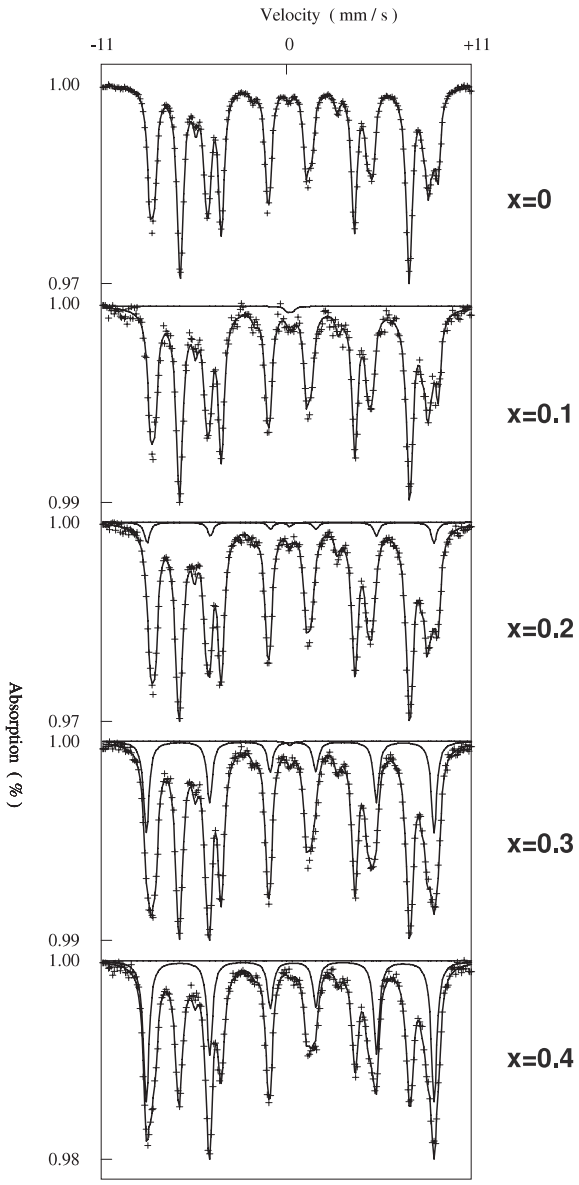

Figure 5. Room temperature Mössbauer spectra of the $Sr_{1-x}Nd_xFe_{12}O_{19}$ powders for the indicated compositions. Both paramagnetic and magnetic contributions are displayed. The magnetic contribution refers to α-Fe_2O_3 and $NdFeO_3$ secondary phases. The paramagnetic contribution refers to (Sr, Nd)$FeO_{3-\varepsilon}$.

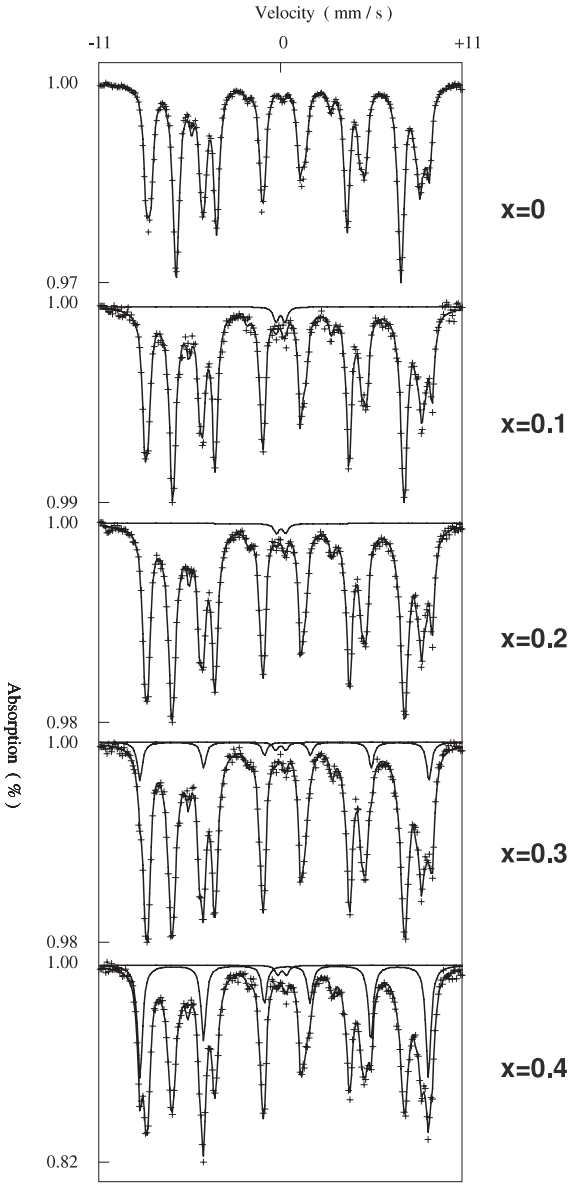

Figure 6. Room temperature Mössbauer spectra of the $Sr_{1-x}Nd_xFe_{12-x}Co_xO_{19}$ powders for the indicated compositions. Both paramagnetic and magnetic contributions are displayed. The magnetic contribution refers to α-Fe_2O_3, $NdFeO_3$ and $CoFe_2O_4$ secondary phases and the paramagnetic contribution refers to (Sr, Nd)$FeO_{3-\varepsilon}$.

spectra were fitted according to the results of the x-ray diffraction analysis. The contributions of the extra phases are displayed in the figures.

The Mössbauer contributions of α-Fe_2O_3, $PrFeO_3$, $NdFeO_3$ and $CoFe_2O_4$ are magnetic at room temperature. As it is very difficult to separate the magnetic contributions of these phases which, moreover, are present in low proportions in the powders, their contributions were fitted by using only one magnetic component, with an isomer shift $\delta = 0.26 \pm 0.04$ mm s^{-1} and a hyperfine field $B = 51.6 \pm 0.03$ T. In some spectra, a paramagnetic component was fitted, with an isomer shift $\delta = 0.07 \pm 0.08$ mm s^{-1} and a quadrupolar splitting $\Delta = 0.55 \pm 0.05$ mm s^{-1}. This contribution was not detected in XRD patterns. It is attributed to Sr-rich (Sr, RE)$FeO_{3-\varepsilon}$ phases [16], whose XRD patterns are similar to those of the corresponding $REFeO_3$ phases.

The relative intensities of the contributions of the extra phases (both paramagnetic and magnetic components) are reported in figure 9(a). It appears that the relative intensities of the extra phases are lower for the Co-containing powders (continuous lines) than for the Co-free powders (dotted lines). This confirms that the presence of Co reduces the proportion of the extra phases in the powders, and thus improves the solubility of the rare earth ion in the M-type hexaferrite. As can be seen in this figure, the total relative intensity of the secondary phases (both magnetic and paramagnetic) is lower in the $x = 0.4$ Pr–Co sample (5.5%) than in the $x = 0.4$

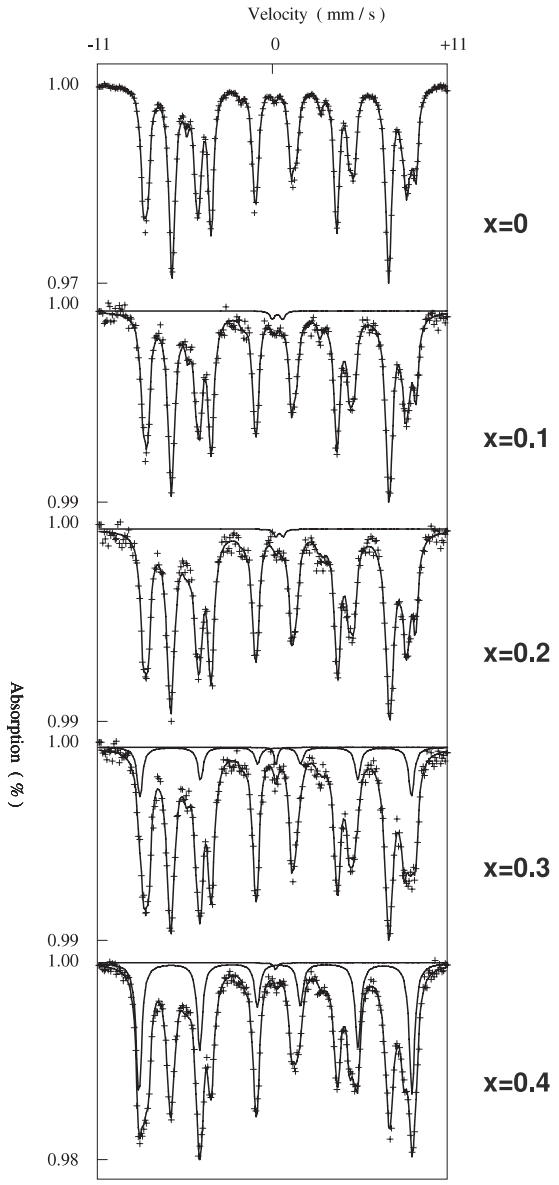

Figure 7. Room temperature Mössbauer spectra of the $Sr_{1-x}Pr_xFe_{12}O_{19}$ powders for the indicated compositions. Both paramagnetic and magnetic contributions are displayed. The magnetic contribution refers to α-Fe_2O_3 and $PrFeO_3$ secondary phases. The paramagnetic contribution refers to (Sr, Pr)$FeO_{3-\varepsilon}$.

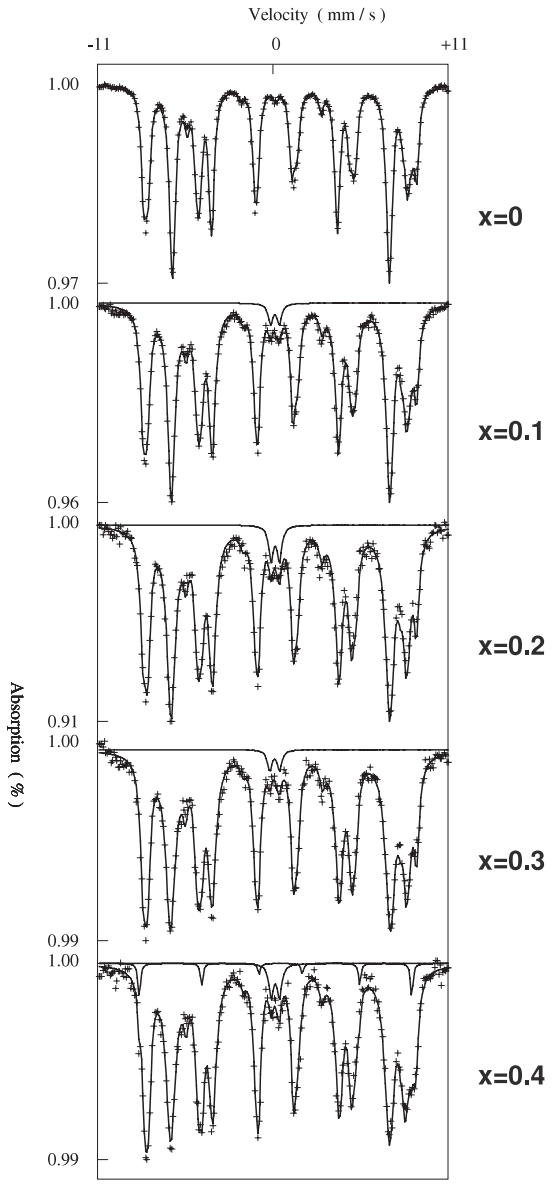

Figure 8. Room temperature Mössbauer spectra of the $Sr_{1-x}Pr_xFe_{12-x}Co_xO_{19}$ powders for the indicated compositions. Both paramagnetic and magnetic contributions are displayed. The magnetic contribution refers to α-Fe_2O_3, $PrFeO_3$ and $CoFe_2O_4$ secondary phases and the paramagnetic contribution refers to (Sr, Pr)$FeO_{3-\varepsilon}$.

Nd–Co sample (21.1%). This indicates that the proportion of secondary phases is lower in Pr–Co hexaferrite powders than in Nd–Co hexaferrite powders. This result confirms that the solubility of Pr is much higher than that of Nd in Co-containing samples. It is worth mentioning that the $x = 0.4$ Pr–Co samples are nearly single phase, as for $x = 0.4$ La–Co samples.

The insertion of rare earth ions in the M-type phase was followed by Mössbauer spectrometry looking at the variations of the hyperfine field of the 12k contribution. It must be noted that the Mössbauer contribution of Fe^{3+} ions in the 12k site is the major contribution to the spectrum. Moreover, in the room temperature Mössbauer spectrum, this contribution is not perturbed by the presence of the contributions of the extra phases, so that its hyperfine field can be measured accurately. In a previous paper, such a measurement was used to explain the variation of the curvature of the magnetization curve in La–Co-substituted $SrFe_{12}O_{19}$ powders [11]. The x dependence of the 12k hyperfine field is shown in figure 9(b) for all the samples. For a given composition, the 12k hyperfine field obtained for the Nd-containing samples is higher than for the Pr-containing samples, suggesting that the presence of the Nd^{3+} ions in the M-type structure has a more pronounced effect on the magnetization than the Pr^{3+} ions. The same tendency is observed for Co-containing samples compared to Co-free samples. All the curves show an increase of the 12k hyperfine field, followed by a plateau. This effect is clearly

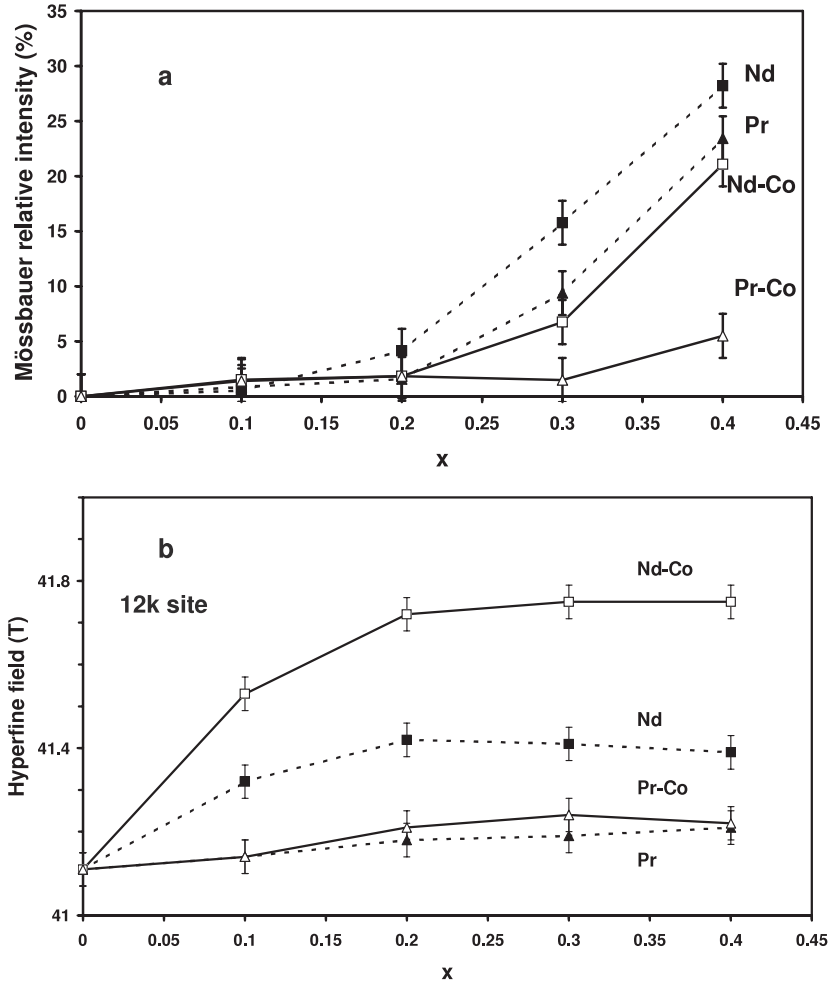

Figure 9. Mössbauer relative intensities of the contributions of the secondary phases (a) and hyperfine field of the 12k site Mössbauer contribution (b) obtained from the $Sr_{1-x}Nd_xFe_{12}O_{19}$, $Sr_{1-x}Nd_xFe_{12-x}Co_xO_{19}$, $Sr_{1-x}Pr_xFe_{12}O_{19}$ and $Sr_{1-x}Pr_xFe_{12-x}Co_xO_{19}$ spectra, as a function of x. The values of the Mössbauer relative intensities of the secondary phases correspond to the sum of both magnetic and paramagnetic contributions.

observed for the Nd-containing samples. It has to be noted that the beginning of the plateau corresponds systematically to the composition from which the relative intensity of the secondary phases strongly increases. This indicates that the maximum rare earth substitution rate leading to single phase hexaferrite samples corresponds to the maximum rare earth substitution rate in the M-type phase.

3.2. Influence of the nature of the rare earth on the solubility of rare earth ions

As shown in figure 9(a), the percentage of secondary phases is higher for Nd substituted samples than for Pr substituted samples. So, it is clear that Pr^{3+} enters the M-type phase more easily than Nd^{3+}. We can thus estimate the maximum substitution rate leading to single phase hexaferrite samples as approximately $x = 0.3$ and 0.2 for the Pr^{3+} and Nd^{3+} ions, respectively, for the processing conditions used. This rate was found to be lower than $x = 0.1$ for the Sm^{3+} ion [4]. These substitution rates, obtained in $SrFe_{12}O_{19}$ hexaferrites after calcination at 1250 °C, are close to those obtained by Deschamp and Bertaut [17] in $BaFe_{12}O_{19}$ hexaferrites which are 0.7, 0.4, 0.3, 0.1 and 0.1, for $La^{3+}Pr^{3+}$, Nd^{3+}, Sm^{3+} and Eu^{3+}, respectively, after calcination at 1400 °C. Thus, for a given calcination temperature, it appears that the maximum solubility of the rare earth ion in the hexaferrite phase is strongly dependent on the nature of the rare earth.

3.2.1. Light rare earths and heavy rare earths. Numerous investigations have been reported in the literature for $(Sr, RE)Fe_{12}O_{19}$ and $(Ba, RE)Fe_{12}O_{19}$ hexaferrites where RE is a light rare earth. However, to our knowledge, no investigation for $(Sr, RE)Fe_{12}O_{19}$ or $(Ba, RE)Fe_{12}O_{19}$ hexaferrites where RE is a heavy rare earth has been reported. This is probably due to the fact that the M-type structure does not favour the introduction of a heavy rare earth. It is worth mentioning that saturation magnetization measurements performed on sintered $Sr_{0.8}RE_{0.2}Fe_{11.8}Co_{0.2}O_{19}$ (RE = La, Pr, Nd, Sm, Gd, Dy, Ho, Y) hexaferrites suggest that the M-type phase is not formed with Gd, Dy, Ho or Y [1].

According to Deschamp and Bertaut, the introduction of La, Pr, Nd, Sm or Eu in $BaFe_{12}O_{19}$ occurs simultaneously

with a variation of the a and c lattice parameters [17]. For the maximal substitution rates, the decrease of c is close to 0.5% for La, Pr, Nd and close to 0.3% for Sm and Eu. The decrease of a is lower than 0.2% for the maximal substitution rates of these five rare earths. In the same article, the authors observed that in the $BaTiO_3$ perovskite structure, Ba can be substituted for a rare earth and Ti for a transition metal, the lattice deformation increasing as the radius of the rare earth decreases. They concluded that the substitution of Ba for a rare earth is more difficult when the radius of the substituting ion is low, thus excluding heavy rare earths.

The influence of the nature of the rare earth on the formation of rare earth containing iron oxides has been shown in garnets as well. Garnets have a $A_3B_2Si_3O_{12}$-type cubic structure [18]. These structures have been the subject of numerous substitutions studies, using rare earths, leading to $RE_3Fe_2Fe_3O_{12}$ type garnets. It has been shown that the rare earth ions are soluble in the garnet structure and that the lattice constant decreases from 1.254 to 1.228 nm as one goes from Sm to Lu [19]. In contrast, limited substitution rates are observed when two rare earth ions are associated in substituted $RE_{3-x}M_xFe_2Fe_3O_{12}$ (M = Pr, Nd and RE = Y, Sm, Eu, Gd, Tb, Dy, Ho, Er, Tm, Yb, Lu) garnets. The association of two rare earth ions limits their solubility in the garnet. The Sm–Nd (or Pr) association in the garnet is more difficult to obtain (the maximal substitution rate of Nd^{3+} or Pr^{3+} in Sm garnets is 0.4 and 0.3, respectively) than Gd–Nd (or Pr) ($x = 1.3$, 0.9) or Ho–Nd (or Pr) ($x = 1.9$, 1.3) associations.

3.2.2. Electronic structure. The M-type hexaferrite phase can be obtained either with bigger (Ba^{2+}, Pb^{2+}) or smaller (Ca^{2+}) cations than Sr^{2+}, the ionic radii of Ba^{2+}, Pb^{2+}, Sr^{2+} and Ca^{2+} ions being equal to 0.135, 0.120, 0.113 and 0.095 nm, respectively. The ionic radius of the 3+ rare earth ions decreases from 0.111 nm (Ce^{3+}) to 0.094 nm (Yb^{3+}), being equal to 0.109, 0.108 and 0.104 nm for Pr^{3+}, Nd^{3+} and Sm^{3+}, respectively. The fact that it is possible to synthesize the M-type phase with ions smaller than Sr^{2+} (Ca^{2+} for example [20, 21]) indicates that the maximum solubility of the rare earth ions in the M-type phase is not determined just by the size of their ionic radius. The electronic structure of the rare earth has to be considered.

The 4f electronic charge distribution is notably different from one rare earth to the other. The α_J second order Stevens coefficient characterizes the asphericity of the 4f shell. Thus, when α_J is positive, the shape of the electronic distribution is prolate [22] (as for Sm), and when α_J is negative, it is oblate [22] (as for Pr, Nd, Ce), as shown in figure 10. α_J is equal to -2.10×10^{-2}, -0.64×10^{-2} and $+4.13 \times 10^{-2}$ for Pr^{3+}, Nd^{3+} and Sm^{3+}, respectively [23]. α_J is thus lower for Pr^{3+} than for Nd^{3+}, leading to a more oblate electronic distribution for Pr^{3+} than for Nd^{3+}.

The fact that the solubility of Pr^{3+} and Nd^{3+} in the $SrFe_{12}O_{19}$ phase is higher than the solubility of Sm^{3+} shows that the substitution of Sr^{2+} by a rare earth ion is made easier if the rare earth 4f charge distribution is oblate than if it is prolate. Thus it appears that in hexaferrites the Sr^{2+} surroundings favour an oblate electronic distribution. The Pr^{3+} Stevens coefficient being three times lower than the Nd^{3+} Stevens coefficient, the solubility of Pr^{3+} must be higher than that of Nd^{3+} ion. This is what is experimentally observed.

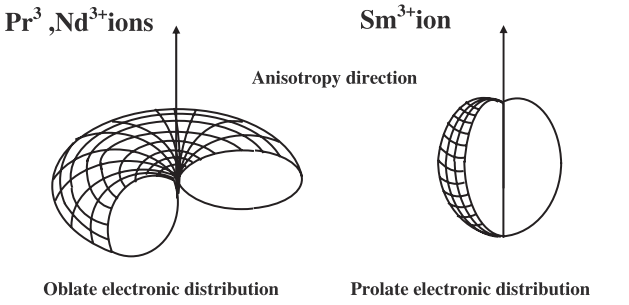

Figure 10. 4f charge distribution for tripositive rare earth ions characterizing a prolate distribution ($\alpha_J > 0$ for Sm^{3+} ion) and an oblate distribution ($\alpha_J < 0$ for Pr^{3+} and Nd^{3+}). α_J is lower for the Pr^{3+} ion than for the Nd^{3+} ion, leading to a more oblate charge distribution.

The numerous studies made with the La^{3+} ion [24–26], the Pr^{3+} ion [26, 27], the Sm^{3+} ion [28] and the Gd^{3+} ion [29] show evidence for the complete solubility of La^{3+} (up to $x = 1$), and the partial solubility of the rare earth ions (lower than $x = 0.4$) in the M-type phase. As the La^{3+} ion does not carry a magnetic moment (this element has no 4f electron), unlike the rare earths, it could be possible that the fact that a rare earth carries a magnetic moment is detrimental to the introduction of a rare earth ion in the M-type structure.

The M-type hexaferrite phase is formed during calcination in the 1100–1400 °C temperature range. At these temperatures, the rare earth ions keep the anisotropic or isotropic character of their 4f electronic charge distribution [30]: oblate for Pr^{3+} and Nd^{3+}, prolate for Sm^{3+} and spherical for Gd^{3+} ($\alpha_J = 0$). Thus a rare earth ion still carries a magnetic moment at the calcination temperature.

Consequently, it appears that the possibility to substitute a rare earth for a Sr^{2+} ion is determined by the electronic structure of the rare earth ion, through the 4f electronic charge distribution, the existence of a magnetic moment and the size of the ionic radius. As the Sr^{2+} site favours rare earth ions with an oblate 4f electronic charge distribution, and according to the fact that the heavy rare earths do not enter the M-type phase, the most favourable rare earth elements that can be introduced in the M-type structure are Pr and Nd.

3.2.3. Synthesis parameters. The synthesis parameters of the M-type hexaferrite phase could be optimized to increase the solubility of the rare earths. However, it has been shown that La is the only element of the lanthanide series that could have been completely substituted for Sr by optimizing the calcination temperature [17]. The optimum calcination temperature for $LaFe_{12}O_{19}$ is 1400 °C: a higher temperature leads to the formation of $LaFeO_3$ and Fe_3O_4 phases, and a lower temperature leads to the formation of $LaFeO_3$ and Fe_2O_3 phases [31]. An optimization of the calcination temperature would probably allow further improvement in the solubility of the Pr and Nd phases in the M-type phase, but the

Table 2. Number of nearest Fe^{3+} and Sr^{2+} neighbours and corresponding mean distances (in nm) for each Fe^{3+} site in the crystal structure of the M-type phase in $SrFe_{12}O_{19}$ [33, 34].

Site	12k	$4f_1$	$4f_2$	2a	2b	Sr
12k	4 0.290	3 0.357	2 0.349	1 0.305	1 0.377	1 0.365
$4f_1$	9 0.357	3 0.362	–	3 0.345	–	–
$4f_2$	6 0.349	–	1 0.272	—	3 0.366	3 0.366
2a	6 0.305	6 0.345	–	–	–	–
2b	6 0.377	–	6 0.366	–	–	3 0.340
Sr^{2+}	6 0.365	–	6 0.366	–	3 0.340	–

electronic structure of Pr and Nd, although favourable to a partial substitution for Sr, seems to be unfavourable for the formation of completely substituted $PrFe_{12}O_{19}$ or $NdFe_{12}O_{19}$ compounds.

3.3. Influence of the presence of Co on the solubility of rare earth ions

The results of both XRD and Mössbauer analyses show that the percentage of secondary phases is much lower in Co-containing samples than in Co-free samples. It remains lower in Pr–Co samples than in Nd–Co samples. This shows that the Pr^{3+} and Nd^{3+} ions enter the M-type phase more easily with Co^{2+} present than without Co^{2+}, the maximum substitution rate leading to single phase hexaferrite samples remaining higher for the Pr^{3+} ion (close to $x = 0.4$) than for the Nd^{3+} ion (close to $x = 0.3$).

Introducing the Co^{2+} ion instead of the Fe^{3+} ion allows compensation for the excess positive charges due to the replacement of Sr^{2+} by Nd^{3+} or Pr^{3+} ions. One could consider that the substitution of Co^{2+} for Fe^{3+} favours the introduction of more rare earth ions in the M-type structure for charge compensation reasons. However, in the M-type cell the charge compensation can occur without the presence of Co^{2+}: a complete change of the valence state of iron ions in the 2a site from Fe^{3+} to Fe^{2+} has been observed in the $LaFe_{12}O_{19}$ compound [31, 32].

The introduction of Co^{2+} ions modifies the surroundings of the rare earth ion, because some Co^{2+} ions occupy Fe^{3+} ion sites that are close to the rare earth site. The closest sites of the Sr^{2+} ion site are 12k, $4f_2$ and 2b (see table 2) [33, 34]. The 2b sites are located in the same plane as Sr^{2+} ions (distance 0.340 nm), the $4f_2$ and 12k sites are located in adjacent planes, at about the same distance from Sr^{2+} (0.366 and 0.365 nm, respectively) (figure 11). The fact that Co^{2+} ions enter the $4f_2$ site can thus be related to the increase in the rare earth solubility in the M-type phase.

The positive influence of Co on the rare earth solubility can be explained by the fact that the presence of a Co^{2+} ion in the $4f_2$ site produces a deficit of positive charges in the surroundings of the rare earth site and thus an increase of the negative charges effect. The potential box that characterizes

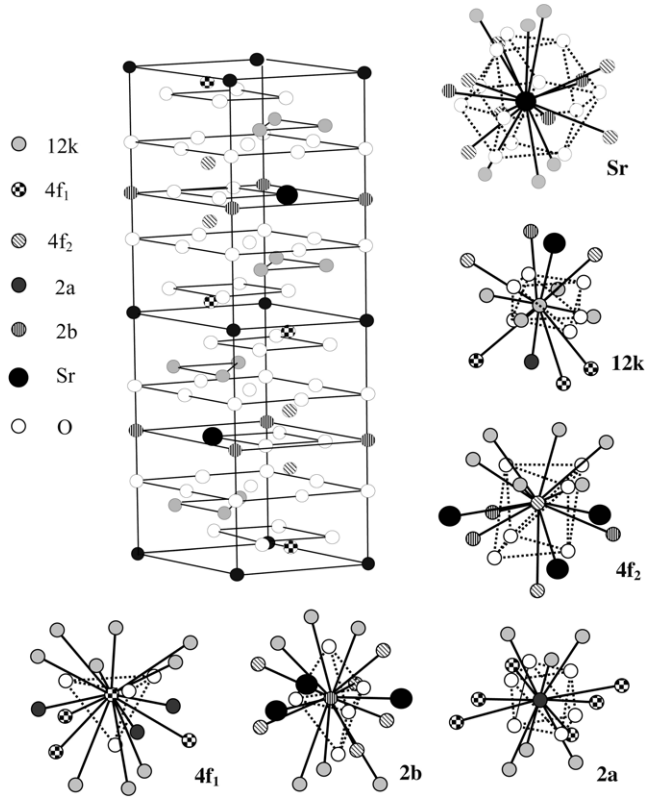

Figure 11. Crystal structure of the hexagonal M-type phase. The Sr site and the five Fe sites with their surroundings are displayed.

the surroundings of the rare earth site is thus more oblate than when no Co^{2+} ion is present in the structure. This should make the solubility of rare earth ions with oblate electronic distributions easier.

4. Conclusion

The structural investigation of $Sr_{1-x}RE_xFe_{12}O_{19}$ and $Sr_{1-x}RE_xFe_{12-x}Co_xO_{19}$ (RE = Pr, Nd) M-type hexaferrite powders with ($x = 0.1, 0.2, 0.3, 0.4$) synthesized by a conventional ceramic process under the same conditions show that the solubility of the rare earth ion in the M-type phase depends on both the nature of the rare earth and the presence of Co. The maximum substitution rates are 0.3 and 0.2 for Pr^{3+} and Nd^{3+} ions, respectively, in Pr and Nd samples and close to 0.4 and 0.3 for Pr^{3+} and Nd^{3+} ions, respectively, in Pr–Co and Nd–Co samples. The solubility of rare earth ions in the M-type hexaferrite phase thus depends on both the nature of the rare earth and the presence of Co.

It appears that the M-type structure does not favour the introduction of a heavy rare earth. Only light rare earths can enter the structure, with a solubility that is related to the shape of the charge distribution of the 4f electrons and to its surroundings in the crystal structure. Rare earth ions are located in the Sr^{2+} site, whose surroundings favour an oblate electronic distribution. Thus, Pr and Nd can enter the M-type structure, and this is not the case for Sm. Co^{2+} ions modify the surroundings of the Sr^{2+} site, improving the introduction

of rare earth ions with oblate electronic distributions. The presence of Co thus increases the solubility of Pr and Nd.

Acknowledgment

The authors are grateful to Dr M B Lepetit (Crismat, Caen) for helpful discussions.

References

[1] Taguchi H, Minachi Y, Masuzawa K and Nishio H 2000 *Proc. 8th Int. Conf. on Ferrites (Kyoto)* ed M Abe and Y Yamazaki, p 405
[2] Kools F, Morel A, Tenaud P, Rossignol M, Isnard O, Grössinger R, Le Breton J M and Teillet T 2000 *Proc. 8th Int. Conf. on Ferrites (Kyoto)* ed M Abe and Y Yamazaki, p 437
[3] Grössinger R, Tellez Blanco J C, Kools F, Morel A, Rossignol M and Tenaud P 2000 *Proc. 8th Int. Conf. on Ferrites (Kyoto)* ed M Abe and Y Yamazaki, p 428
[4] Lechevallier L, Le Breton J M, Wang J F and Harris I R 2004 *J. Magn. Magn. Mater.* **269** 192
[5] Tellez Blanco J C, Grössinger R, Müller M, Küpferling M, Wiesinger G, Wang J F, Ponton C B and Harris I R 2000 *Proc. Int. Work. on Rare Earth Magnets and Their Applications (Newark)* ed G C Hadjipanayis and M J Bonder p 192
[6] Mocuta H, Lechevallier L, Le Breton J M, Wang J F and Harris I R 2004 *J. Alloys Compounds* **364** 48
[7] Sharma P, Verma A, Sidhu R K and Pandey O P 2003 *J. Alloys Compounds* **361** 257
[8] Kubota Y, Takami T and Ogata Y 2000 *Proc. 8th Int. Conf. on Ferrites (Kyoto)* ed M Abe and Y Yamazaki, p 410
[9] Gorter E W 1954 *Philips Res. Rep.* **9** 403
[10] Morel A, Le Breton J M, Kreisel J, Wiesinger G, Kools F and Tenaud P 2002 *J. Magn. Magn. Mater.* **242** 1405
[11] Le Breton J M, Teillet J, Wiesinger G, Morel A, Kools F and Tenaud P 2002 *IEEE Trans. Magn.* **38** 2952
[12] Teillet J and Varret F 1983 MOSFIT program (unpublished)
[13] Rensen J G, Schulkes J A and Van Wieringen J S 1971 *J. Physique Coll.* **32** C1 924
[14] Evans B J, Grandjean F, Lilot A P, Vogel R H and Gerard A 1987 *J. Magn. Magn. Mater.* **67** 123
[15] Lechevallier L, Le Breton J M, Wang J F and Harris I R 2004 *J. Phys.: Condens. Matter* **16** 5359
[16] Uhm Y R, Sur J C and Kim C S 2000 *J. Magn. Magn. Mater.* **215/216** 554
[17] Deschamps A and Bertaut F 1957 *C. R. Acad. Sci.* **17** 3069
[18] Guillot M, Le Gall H and Leblanc M 1990 *J. Magn. Magn. Mater.* **86** 13
[19] Geller S 1967 *Z. Kristallogr.* **125** 1
[20] Asti G, Carbucicchio M, Deriu A, Lucchini E and Slaokar G 1980 , *J. Magn. Magn. Mater.* **20** 44
[21] Buijs 1987 *Philips Trainee Report* Eindhoven
[22] Coehoorn R L 1991 *Supermagnets Hard Magnetic Materials* ed G J Long and F Grandjean (Dordrecht: Kluwer) chapter 8
[23] Coey J M D 1996 *Rare Earth Iron Permanent Magnets* ed J M D Coey (New York: Oxford Science) chapter 1
[24] Liu X, Zhong W, Yang S, Yu Z, Gu B and Du Y 2002 *J. Magn. Magn. Mater.* **238** 207
[25] Küpferling M, Grössinger R, Pieper M W, Wiesinger G, Michor H, Ritter C and Kubel F 2006 *Phys. Rev.* B **73** 144408
[26] Ounnunkad S 2006 *Solid State Commun.* **138** 472
[27] Wang J F, Ponton C B and Harris I R 2005 *J. Alloys Compounds* **403** 104
[28] Wang J F, Ponton C B and Harris I R 2006 *J. Magn. Magn. Mater.* **298** 122
[29] Litsardakis G, Manolakis I and Efthimiadis K 2007 *J. Alloys Compounds* **427** 194
[30] NIST 2007 *Atomic Spectra Database Levels Data* (version 3.1.3) online
[31] Lotgering F K 1974 *J. Phys. Chem. Sol.* **35** 1633
[32] Sauer C, Köbler U, Zinn W and Stäblein H 1978 *J. Phys. Chem. Solids* **39** 1197
[33] Wartewig P, Krauze M K, Esquinazi P, Rösler S and Sonntag R 1999 *J. Magn. Magn. Mater.* **192** 83
[34] Obradors X, Solans X, Collomb A, Samaras D, Rodriguez J, Pernet M and Font-Altaba M 1988 *J. Solid State Chem.* **72** 218